REPORT DOCUMENTATION PAGE

Form Approved
OMB NO. 0704-0188

1. AGENCY USE ONLY (Leave Blank)	2. REPORT DATE May 20, 1999	3. REPORT TYPE AND DATES COVERED Final Progress Report for 6/15/95 to 12/31/98

4. TITLE AND SUBTITLE
Application of Near-Field Optics to Semiconductor Materials Characterization

5. FUNDING NUMBERS
DAAH04-95-1-0368

6. AUTHOR(S)
Prof. Robert D. Grober

7. PERFORMING ORGANIZATION NAME(S) AND ADDRESS(ES)
Yale University
155 Whitney Avenue, P.O. Box 208337
New Haven, CT 06520

8. PERFORMING ORGANIZATION REPORT NUMBER

9. SPONSORING / MONITORING AGENCY NAME(S) AND ADDRESS(ES)

U. S. Army Research Office
P.O. Box 12211
Research Triangle Park, NC 27709-2211

10. SPONSORING / MONITORING AGENCY REPORT NUMBER

ARO 34570.4-MS-YIP

11. SUPPLEMENTARY NOTES
The views, opinions and/or findings contained in this report are those of the author(s) and should not be construed as an official Department of the Army position, policy or decision, unless so designated by other documentation.

12 a. DISTRIBUTION / AVAILABILITY STATEMENT

Approved for public release; distribution unlimited.

12 b. DISTRIBUTION CODE

13. ABSTRACT (Maximum 200 words)

This grant supported a program for local spectroscopic stsudies of semiconductor nanostructure materials. Our work has looked at the various types of techniques of near-field optics and pursued the options that are optimized for the optical spectroscopy of semiconductor nanostructures. The thrust of the research has involved the use of solid immersion lenses. This form of near-field optics strikes a balance between the need for high spatial resolution and high optical through put. We have demonstrated that these techniques can be implemented within the context of a cryogenic system and obtain spatial resolution of order $\lambda/3$.

We have used these techniques to characterize naturally occuring quantum dots in thin GaAs quantum wells. Our studies reveal the surprising fact that these samples have not only zero dimensional excitons but also two dimensional excitons. In fact, most of the material plays host to the two dimensional species while the zero dimensional species occupies only 1-3% of the sample. This result is surprising because all of the light emission comes from the zero dimensional exciton. The two dimensional exciton is observed using photoluminescence excitation diffusion, a technique wherein we are able to generate a local optical excitation and watch it diffuse.

14. SUBJECT TERMS
Near-Field Optics, Imaging Spectroscopy, Hyperspectral Imaging, Quantum Dot, Excitons

15. NUMBER OF PAGES

16. PRICE CODE

17. SECURITY CLASSIFICATION OR REPORT	18. SECURITY CLASSIFICATION ON THIS PAGE	19. SECURITY CLASSIFICATION OF ABSTRACT	20. LIMITATION OF ABSTRACT
UNCLASSIFIED	UNCLASSIFIED	UNCLASSIFIED	UL

NSN 7540-01-280-5500

Standard Form 298 (Rev.2-89)
Prescribed by ANSI Std. 239-18
298-102

REPORT DOCUMENTATION PAGE (SF298)
(Continuation Sheet)

The research funded by this grant involves the use of near-field optics for the characterization of nanostructured semiconductor materials. This final report highlights the most important results of the research suppported by this grant, including both advances in instrumentation and the results the studies of naturally occuring quantum dots in narrow GaAs quantum wells. The details of this research are described in the papers listed at the end of this report.

Instrumentation

Optical Apertures

We continued to develop the techniques of aperture based near-field optics. Our research began with a theoretical analysis of the electromagnetic fields associated with small optical apertures [1]. We then pursued a new fabrication technique, where an aperture is fabricated on the end of a optical fiber using a chemical etching technique [3]. We documented that this technique yielded a thousand fold increase in the amount of light one obtains from the aperture, yielding microwatts from l/10 sized apertures. This is a central issue for our field, as the losses associated with traversing a sub-wavelength sized optical aperture remains as the largest single drawback of this technique.

Tuning Fork based Shear Force Feedback

Another very important aspect of aperture based near-field optics is the ability to position the aperture in close proximity to the sample without touching the sample. Our research continued the development of tuning fork based shear-force feedback. This technique uses a conventional tuning fork quartz oscillator as the force sensor. These tuning fork oscillators are used commercially for keeping time. We have pushed this technology to its fundamental limits [8] and determined that at room temperature these quartz sensors can measure forces as small as 0.4 pN/$\sqrt{\text{Hz}}$ and root mean square (RMS) displacements as small as 0.2 pm.

Traditional force sensing for scanned probe microscopy (SPM) uses Si cantilevers. This sensor has evolved quite naturally out of the MEMS community, which is focuses on Si materials systems. Our use of quartz tuning forks as force sensors raises the issue of which material system makes for the best SPM force sensor: Si, quartz, or something else. If one simply views a force sensor as a very high Q oscillator, the best such systems are made out of quartz. Our work is the first to explore this new application of quartz and we expect that it will evolve into a new research direction for our laboratory.

Antenna for Near-Field Optics

We explored the possibility that one could achieve enhansed spatial resolution using optical antenna as opposed to optical apertures [2]. We documented that this works excellently for GHz based systems. Our unpublished results in the visible optical spectrum showed that this technique is not as promising as it is for GHz radiation. The reason is that metals (i.e. the material out of which antenna are built) do not function as metals as one gets close to the plasma frequency. For aluminum in particular, the currents driven in the metal in response to the incoming visible radiation are phase shifted by 7 degrees and only 90-95 percent as large as for GHz radiation. This reduction in amplitude and shift in phase destroys the perfect destructive interference effects requried to achieve the very high spatial resolution obtained with the GHz antenna system. Considering the known dielectric constants of Aluminum and Gold, we suggest that antenna based near-field optical microscopes would be useful at wavelengths as short as 5 microns.

We filed a patent based on these findings [4]. The patent is awarded under patent number 5,696,372 and is titled "High efficiency near-field electromagnetic parobe having a bowtie antenna structure."

Solid Immersion Lens

As stated above, even the best chemically etched near-field optical apertures have a throughput of only 1 part in 1000. This can be a large drawback for experiments that require operation at very low light levels. There are applications where a compromise between small spot size and high throughput is required. The vehicle for this compromise is the solid immersion lens (SILs). This optic is very similar to the conventional oil immersion lens in that light converging on a sample propagates through a material of high refreactive index, n, enhansing the spatial resolution by n. While immersion oils have n as large as 1.5, SILs offer much larger n. For instance, sapphire SILs have been made with n=1.76 and GaP SILs are in development with n=3.4.

We have spent considerable effort to develop the use of SILs for imaging spectroscopy of semiconductors in cryogenic environments [6]. The experimental work described below uses a sapphire SIL and exemplifies the importance of the comprimise between spot size and throughput. We plan to continue our work in this field. In particular, we are working with Digital Instruments to develop GaP based SILs.

Imaging Spectroscopy of 0D and 2D Excitions in Narrow GaAs Quantum Wells

We have worked collaboratively with Dan Gammon at Naval Research Laboratories to study the excitonic landscape in narrow GaAs quantum wells [5,7]. While this physical system has not changed much in the last 5-10 years, our understanding of it has evolved everytime a new characterization technique is used. Narrow GaAs quantum wells were first grown in an attempt to realize two dimensional (2D) excitons. The original papers observed confinement effects consistent with 2D excitons. They also observed that there were usually at least two peaks associated with these wells, corresponding to quantum wells differing in well width by only a monlayer. These initial studies performed spectroscopy without any form of imaging. About five years ago people began characterizing this materials system using spectroscopic imaging. They found that the excitions in these systems were not 2D but were actually 0D, confined in quantum dots formed by lateral imperfections in the heterojunctions that define the quantum well. These studies were conducted both with far-field microscopy (i.e. spatial resolution of order 1.5 μm) and with near-field optical apertures (spatial resolution of order 0.1 μm).

We have studied these samples using SIL microscopy. While this technique is only capable of spatial resolution of order 0.25 μm, which is 2-3 times larger than that of aperture optics, the throughput is at least a thousand fold larger. This particular compromise is perfect for this study because while the spatial resolution is high enough to isolate individual dots, the increase in throughput allows us both to take much more data and study the system at much lower excitation densities. We use a scanning confocal imaging technique where either an emission or abosrption spectrum is taken at each point in the image. The data is analyzed using techniques similar to that of hyperspectral imaging. Our studies revealed the following facts about the system:

1) All of the emission from the sample is local, consistent with the previous imaging experiments and the concept that the emitting excitons are confined in quantum dots.

2) The quantum dots organize themselves into two distinct groups. These groups anticorrelate both spectrally and spatially. We interpret this to mean that the quantum well has regions that are on average 10 monolayers thick and regions that are 9 monolayers thick. These regions anticorrelate, yielding what can be described as islands. The concept of islands is consistent with the earliest far-field studies of these samples.

3) Most of the sample does not emit light. Only 1-3% of the sample consists of light emitting quantum dots. One can think of the quantum dots as imperfections within the monolayer islands. We believe that the imperfections are lateral defects in the heterojunctions that define the quantum well.

4) The dark regions of the sample all exhibit the same absorption line. We have assigned this line to a 2D exciton which exists in the material that defines the lateral barrier of the dot. Our experiments probed this absorption line using the technique of photoluminescence excitation diffusion. It involves pumping exciatations into the system and watching them diffuse to emission centers. We have directly mapped the diffusion of these 2D excitions and found that they have a maximum diffusion length of order 0.5 microns but that the diffusion is defined by the surrounding energy landscape.

5) The emission spectrum of these samples evolves from independent quantum dots to an electron-hole plasma as the pump intensity it turned up. The plasma density is spatially inhomogeneous, as our data shows that

the plasma grows out from the dots and eventually fills in the entire sample. In our experiments, the low intensity limit of single excitons emitting from quantum dots can only be achieved using the solid immersion lens. Both the far-field and near-field technqiues do not have the collection efficiency to study the system in the low excitation limit of single excitons.

Future Directions

Our future work will evolve on two fronts. First, we plan to pursue the use of quartz oscillators as force sensors for scanned probe microscopy. We hope to start an effort to nanofabricate the probe directly into the quartz resonantor structure. Second, we will continue our work with spectroscopic imaging of quantum dot systems. However, we will change materials systems as part of a developing collaboration with Prof. Jerry Woodall, who specializes in MBE and who recently joined the Yale University faculty. We plan to study III-V and II-Vi quantum dot systems on GaP and Si substrates with the goal of developing strong visible light emiters.

Published Journal Articles

[1] R.D. Grober, T.Rutherford, and T.D. Harris, *Modal approximation for the electromagnetic field of a near-field optical probe*, Applied Optics **35**(19), 3488 (1996).

[2] R.D. Grober, R.J. Schoelkopf, and D.E. Prober, *The Optical Antenna: Towards a unity efficiency near-field optical probe*, Applied Physics Letters **70**(11), 1354 (1997).

[3] S.J. Bukofsky and R.D. Grober, *Video rate near-field scanning optical microscopy*, Applied Physics Letters **71**(19), 2749 (1997).

Patents

[4] R.D. Grober, R.J. Schoelkopf, and D.E. Prober, *High Efficiency Near-Field Electromagnetic Probe*, U.S. Patent #5696372 (December 1997).

Articles Submitted for Publication

[5] Q. Wu and R.D. Grober, *Imaging Spectroscopy of two-dimensional excitons in a narrow GaAs/AlGaAs quantum well*, submitted to Physical Review Letters. (attached to this report)

Articles in Preparation

[6] Q. Wu and R.D. Grober, *Design of a solid immersion microscope at low temeratures.*

[7] Q. Wu and R.D. Grober, *Electron-hole plasmas in GaAs quantum dots.*

[8] R.D. Grober, J. Acimovic, J. Schuck, D. Hessman, P. Kindlemann and J. Hespanha, K. Karrai, I. Tiemann, and S. Manus, *Fundamental Limits to Force Detection using Quartz Tuning Forks.* (attached to this report)

Fundamental Limits to Force Detection using Quartz Tuning Forks

Robert D. Grober, Jason Acimovic, Jim Schuck, Dan Hessman, Peter Kindlemann, and Joao Hespanha.

Department of Applied Physics, Yale University, New Haven, CT 06520

Khaled Karrai, Ingo Tiemann, and Stephan Manus

Center for NanoScience, Sektion Physik der LMU
Geschwister-Scholl-Platz 1, 80539 Munich, Germany

Abstract:
This paper explores the fundamental limits of the use of quartz tuning forks as force detectors in scanned probe microscopy. It is demonstrated that at room temperature, pressure, and atmosphere these force sensors have a noise floor of 0.4 $\mathrm{pN}/\sqrt{\mathrm{Hz}}$ and exhibit a root mean square Brownian motion of only 0.2 pm. When operated as a shear force sensor both dissipative and reactive forces are detected on approach to the sample. These forces are sufficient to reduce the amplitude of motion of the probe nearly to zero without physically contacting the surface. It is also demonstrated that conventional proportional-integral feedback control yields closed loop responses at least 40 times faster than their open loop response. This result indicates that the mechanical Q of the resonator should always be maximized to obtain the highest force sensitivity and that this does not degrade the response of measurement system.

It is well established that quartz tuning forks can be used as sensors for acoustic and force microscopy [1,2]. Their very high mechanical quality factor Q (10^3 to 10^5) provides a built-in high gain and makes them very sensitive to sub-pN forces when used at or near their resonance frequency (10^4 Hz to 0.5 x 10^6 Hz). Their advantage is that the measurement of their oscillation amplitude uses the piezoelectric effect native to quartz crystals yielding an electric signal proportional to the applied forces [3] and making them small, robust and simple to operate compared to optical force measurement schemes. They have been used as force detectors in near-field optical microscopy [4], atomic force microscopy [5], magnetic force microscopy [6], and magnetometry [7]. This letter is designed to clearly elucidate the fundamental limits associated with the use of these sensors for force microscopy.

The key to implementing tuning forks for force detection is to accurately measure the fundamental resonance of the tuning fork as a function of applied force. This can be done either by shaking the fork at its mechanical resonance and monitoring the induced voltage or by directly driving the tuning fork with a resonant voltage and measuring the induced current. We have chosen to implement the latter, as it provides for a system that is simpler mechanically at the expense of only minimal electronics.

The equivalent circuit for the tuning fork is a series *RLC* resonator in parallel with package capacitance, which is typically of order a few pF. When driving the tuning fork directly with a voltage source, the package capacitance yields both series and parallel

resonances, dramatically distorting the line shape from that of the bare *RLC* resonator. To eliminate the effect of the package capacitance, we use the bridge circuit shown in Fig. 1(a). The transformer yields two wave forms phase shifted from each other by 180 degrees. By appropriately adjusting the variable capacitor, the current through the package capacitance is negated by the current through the variable capacitor.

A standard operational amplifier circuit is used to convert the net current to a voltage. The current to voltage (I-V) gain of the circuit has been calibrated from DC to 100 kHz and is found to be described as $Z_{gain} = R_g \Big/ \sqrt{1+\left(2\pi f R_g C_g\right)^2}$ where f is the frequency, R_g =9.51 MΩ, and C_g =0.24pF is stray capacitance in parallel with R_g. The resulting I-V gain at 32.7 kHz is Z_{gain}=8.42 MΩ. Having calibrated the measurement system, the impedance of the tuning fork can be accurately measured. We measure a bare fork at room temperature, pressure, and atmosphere. White voltage noise is applied to the fork and the resulting output is recorded. The ratio of the output to input is shown as the filled circles in Fig. 1(b). The response fits well to the Lorentzian line shape

$$A\frac{f_0}{Q}f \Big/ \sqrt{(f_0^2 - f^2)^2 + \left(\frac{f_0}{Q}f\right)^2} \qquad (1)$$

with A=17.14, f_0=32773.3 kHz, and Q =8557, shown as the solid line. This result demonstrates that the effect of the package capacitance has been negated and the harmonic oscillator is an excellent model for the response of the tuning fork. Values for the *RLC* circuit model can be determined by comparing the above line shape to the formula for the gain of the amplifier with the *RLC* resonator as the input impedance, yielding $R = Z_{gain}/A$ =0.49 MΩ, $L = RQ/2\pi f_0$ =21 kH, and $C = 1/(4\pi^2 f_0^2 L)$ 1.1 fF. R is large enough that we attribute it completely to mechanical dissipation associated with motion of the quartz.

Another important calibration is the amplitude of oscillation of the tuning fork as a function of the output voltage, which we denote by the parameter α. This has been determined by interferometrically measuring the physical amplitude of oscillation of one arm of the tuning fork while simultaneously measuring the output voltage of the system. This interferometric technique is described in detail elsewhere [8]. Our calibration yields $\alpha = 59.6 \pm 0.1$ pm / mV. Viewing the tuning fork as a current source, it is convenient to write the above equation in terms of the current to voltage converting resistor, $\alpha = \beta/Z_{gain}$, yielding β=0.50 m/A. Because the charge separation in the tuning fork is amplitude dependent, calibration in terms of current yields an accurate measure of the amplitude of motion of the fork.

The fundamental limits of our ability to measure the resonance are defined by the intrinsic system noise. We can determine these limits experimentally by measuring the output noise with the input voltage grounded. The resulting output is shown in Fig 2 as the filled circles. A noise analysis of the circuit shows the two primary noise sources are the Johnson noise of the feedback resistor, $\sqrt{4k_B T R_g}$ V/$\sqrt{\text{Hz}}$, and the Johnson noise associated with mechanical dissipation in the fork, as manifested by the R in the series *RLC* equivalent circuit,

$$\sqrt{4k_BTR}\left(Z_{gain}/R\right)\left(ff_0/Q\Big/\sqrt{(f_0-f^2)^2+\left(ff_0/Q\right)^2}\right)\quad \mathrm{V}/\sqrt{\mathrm{Hz}}\,. \qquad (2)$$

k_B is the Boltzman constant, T is temperature, and all the other parameters have already determined experimentally. These two noise terms add in quadrature. This model has no adjustable parameters and is shown as solid line in Fig. 2. Based on the agreement between the model and the data, we assert enough about the performance of the system is understood to make definitive statements about the fundamental limits to the use of the quartz tuning fork for force measurements. In particular, we address issues related to the minimum detectable displacement, minimum measurable force and maximum measurement speed.

The first issue relates to the minimum detectable displacement of the tuning fork. The power spectrum of the noise associated with the tuning fork [i.e. the square of Eq. (2)] can be integrated so as to obtain the root mean square (rms.) voltage noise, $V_{rms}^2 = 4k_BTR\left(Z_{gain}/R\right)^2\left(\pi f_0/2Q\right)$, which evaluates to V_{rms}=3.8 μV. The interferometric measurement allows us to convert this to an rms displacement, x_{rms}=0.22 pm. This is the random motion of one arm of the fork due to thermal fluctuation.

With this value for x_{rms}, we use the equipartition theorem to calculate an effective spring constant, $k = k_BT/(2x_{rms}^2) \approx 36\ \mathrm{kN/m}$. Note that this differs from the standard cantilever calculation by a factor of two because the thermal energy in a tuning fork is equally distributed between the two cantilevered arms of the fork . We can compare this experimentally determined value of k with the calculated spring constant for one arm of the tuning fork. The theoretical spring constant is obtained from the formula $k = Ewt^3/(4l^3) \approx 47\ \mathrm{kN/m}$ [9], where E=7.87x10^{10} N/m^2 is the Young's modulus of quartz, w=0.5 mm is the width of the fork, t=0.65mm is the thickness of the fork, and l=3.85 is the length of one arm of the fork. Thought the agreement between experiment and theory is not very good, we believe that we understand the discrepancy. Both w and t are determined accurately by breaking the fork and directly measuring their dimensions with a micrometer. The most difficult number to determine is the length, l. The actual fork consists of two cantilevers connected by a cross bar and the intersections are characterized by rounded corners. The value l=3.85 represents the minimum likely length of a cantilever. It is entirely likely that strain fields extend some distance into the cross bar. One would have perfect agreement between the measurement and the calculation if the effective length was l=4.2 mm, only 350 μm larger than the value we measured.

The thermal energy can be thought of in terms of an effective force acting on the tuning fork. This force has a flat power spectrum, S_F, in units of N^2/Hz. One can calculate the power spectrum from the equation [10]:

$$x_{rms}^2 = \int_0^\infty S_F \left| \frac{f_0^2/k}{f_0^2 - f^2 - i(ff_0/Q)} \right|^2 df\,.$$

Evaluating the integral and again using the equipartition theorem, one obtains

$$S_f^{1/2} = \sqrt{2/\pi f_0 Q}\left(k_BT/2x_{rms}\right) = 0.44\ \mathrm{pN}/\sqrt{\mathrm{Hz}}$$

Again, this equation for S_f differs from that for Si cantilevers, now by a factor of four, because the thermal motion is distributed between two cantilevers.

As will be discussed below, it is important to understand the sensitivity to force as a function of bandwidth. The ratio of signal voltage to noise voltage, S/N, as a function of bandwidth, Δf, is given by the expression

$$S/N = \frac{\frac{1}{\beta}\frac{Q}{k}F_s}{\sqrt{4k_BT\frac{1}{R_g}\Delta f + 4k_BT\frac{Q}{Z_r}\int_{\Delta f} df \frac{(ff_0/Q)^2}{\left(f_0^2 - f^2\right)^2 + (ff_0/Q)^2}}} \quad (3)$$

where all terms are written as currents. The numerator is just the response of the system to a resonant force and the denomenator is the quadrature sum of the two noise terms. We have written R as Z_r/Q where $Z_r = \sqrt{L/C}$ is the resonant impedance of the inductive and capacitive terms in the RLC resonator. This equation is useful because it shows directly how S/N scales with Q, R_g, and Δf. The noise is dominated by the resonant impedance of the tuning fork as long as the resonant impedance is significantly less than R_g. This criterion is good out to frequencies of order

$$|f - f_0| \le \frac{f_0}{2Q}\sqrt{\frac{R_g}{Z_r/Q} - 1}.$$

This is clearly seen to be the case in Fig. 2. One would prefer that the noise always be dominated by the thermal noise of the fork; however, as one works at larger bandwidths, the noise associated with R_g becomes dominant. This can be remedied by making R_g larger; however, that degrades the time response of the amplifier due to the stray capacitance, C_g. Ultimately, the choice of R_g is a tradeoff between fast response and large S/N ratio. We believe that R_g ~10MΩ is a reasonable compromise for our system.

Tuning forks are usually used as force sensors by attaching an appropriate probe to one arm of the fork. The measurement is made by resonantly driving the fork with a constant amplitude force and monitoring the response as a function of the height of the probe above the sample. The oscillatory motion of the probe can be either parallel or perpendicular to the surface. In our experiments, the probe oscillates parallel to the surface. As the probe gets closer to the sample both dissipative and reactive forces are experienced by the probe, resulting in a decrease in the amplitude and a change in phase of the tuning fork. It is important that the probe remain stiff at the resonant frequency of the fork to ensure maximum damping of the tuning fork. Shown in Fig. 3(a) is an approach curve for $A\cos\theta$, where A is the amplitude of oscillation and θ is the phase of the oscillation referenced to the phase of the unperturbed (i.e. fully retracted) oscillator. In practice this corresponds to the 'X' output of a lock-in amplifier. This data is taken at room temperature, pressure, and atmosphere with a peak amplitude of 16 pm. The probe is a sharpened gold STM probe and the sample is freshly pealed, highly oriented, pyrolitic graphite. This arrangement allows simultaneous tunneling between the probe and the sample so as to indicate when the probe contacts the surface. The tunneling current is also shown in the Fig. 3(a). The height of the probe above the surface is calibrated using the

onset of tunneling as the indicator of contact between the surface. This data completely rules out the notion [11] that approach curve involves contact between the probe and the surface.

Shown in Fig. 3(b) is Q and f_0 as a function of the height of the probe above the surface. This data was taken open loop, parking the positioning system a fixed distance above the surface and probing the response of the fork. Note that dissipative forces dominate most of the approach while shifts in resonant frequency become important only within a few nanometers of the surface. This fact is crucially important for the analysis that follows. A future paper will discuss the nature of the forces involved in this experiment [12].

The final issue is the speed with which the measurement can follow changes in force. Force images of surfaces are made by operating the system in closed loop feedback and using either amplitude, phase or a combination of the two as the set point for the feedback. When using conventional Si cantilevers it is well known [13] that one must resort to phase sensitive techniques of closed loop feedback in order to make the system respond faster than of the open loop response time of the resonator, $1/\tau = \pi f_0/Q$. These techniques have also successfully been implemented with tuning fork systems [14, 15, 16]. However, we show below that conventional proportional and integral (*PI*) feedback control is sufficient for most uses of tuning forks. We justify this experimental observation with a short theoretical discussion.

The experiment is done at room temperature, pressure and atmosphere. A tapered fiber probe is mounted on the fork consistent with operation in a near-field scanning optical microscope. The open loop response of the loaded tuning fork corresponds to the line shape in Eq. (1) with $f_0/2Q = 8$ Hz and correspondingly $\tau = 20$ msec. The tuning fork is driven at resonance by a voltage source of fixed amplitude and frequency and the resulting current is measured with the circuit of Fig. 1(a). This output is detected with a lock-in amplifier whose phase is referenced to the phase of the resonantly driven tuning fork. The '*X*' output of the lock-in amplifier is fed to conventional *PI* feedback electronics which then adjusts the position of the probe above the surface. The set point of the feedback is adjusted so that the probe is fixed approximately 10 nm above the surface. To test the response of the closed loop system, the vertical position of the sample is intentionally dithered at 100 Hz using a 1 nm square wave. The output of the control electronics, shown in Fig. 4, clearly follows the 100 Hz signal. The rise time of the response is of order 0.5 msec, *40 times faster than the open loop response*. We are unable to go faster and believe the reason is due to resonances in the mechanical positioning system; however, the point is clear: simple *PI* control electronics yield a stable closed loop tracking system that can operate at speeds much faster than the open loop system.

A simple theoretical justification of this experimental result follows. Consider the tuning fork and the lock-in amplifier as a single unit. The lock-in amplifier demodulates the signal from the fork, beating the AC signal to DC. The response function of a harmonic oscillator demodulated at its resonant frequency is a single pole low pass filter with the response $(i/\tau)/(2\pi f + i/\tau)$, where τ is given above. The control system is now that of a classic tracking system where the system to be controlled responds as a single pole low pass filter. This problem is well documented in standard undergraduate texts

[17]. The optimum control electronics for this system uses *PI* feedback electronics. The response function for the closed loop system is proportional to $e^{-\Gamma t}e^{\pm i\Omega t}$. When the relative magnitudes of P and I are optimized to $I = (1+P)^2/2\tau$, the relations $\Gamma = \Omega = (1+P)/2\tau$ are obtained. Note that as P and I are increased the system responds faster and remains stable.

Complications to this simple analysis occur because Q and f_0 are functions of the height of the oscillator above the surface. These complications degrade the maximum achievable response speed only when they introduce additional phase lag in the feedback path. If only the Q of the resonator changes, the tuning fork still demodulates as a single pole low pass filter and no additional phase lag is introduced. As the resonant frequency shifts to $f_0 + \varepsilon$, the demodulated response becomes

$$\frac{1}{2}\left[\frac{i/\tau}{2\pi(f-\varepsilon)+i/\tau}+\frac{i/\tau}{2\pi(f+\varepsilon)+i/\tau}\right].$$

The closed loop response of this system retains the same functional form, $e^{-\Gamma t}e^{\pm i\Omega t}$, with the modification

$$\Gamma = \frac{(1+P)}{2\tau} \text{ and } \Omega \approx \frac{(1+P)}{2\tau}\sqrt{1+\left(2\pi\varepsilon\frac{2\tau}{(1+P)}\right)^2}.$$

This simple analysis shows clearly the origin of the ringing that normally accompanies frequency shifts of the resonator. This ringing is analogous to increasing the integral gain such that the control loop is out of balance. This effect is not important as long as $\varepsilon < (1+P)/(4\pi\tau)$. This condition is $\varepsilon < 300$ Hz in the above experiment, which is satisfied even for the maximum frequency shifts shown in Fig. 3(b). The situation is different for very high sensitivity Si cantilever applications where the dither amplitudes and frequency shifts are larger, and the closed loop bandwidths are purposely small. Clearly, shifts in resonant frequency become a serious problem for these Si cantilevers and solutions involving phase sensitive detection are necessary[18]. However, as is documented above, tuning fork sensors do not suffer these problems and thus simple *PI* control is sufficient.

It is clear that the advantage of having a probe with very high Q is that it allows for measuring very small forces. From the noise analysis above, the signal to noise ratio scales as $Q/\sqrt{\Delta f}$ when measuring with a closed loop response significantly faster than the open loop response. This strongly suggests that one should not aim to reduce the Q of the system in an attempt to scan fast. It is far more efficient to maximize Q and correctly implement the control system. As such the sensitivity to noise increases only as the square root of the bandwidth of the system.

In summary, we have documented some fundamental limits to the use of quartz tuning fork resonators as force detectors in scanned probe microscopy. At room temperature, pressure, and atmosphere these force sensors have a noise floor of $0.4\ \text{pN}/\sqrt{\text{Hz}}$ and experience a root mean square thermal motion of only 0.2 pm. We show the Q should always be maximized to obtain the highest force sensitivity and that this in no way degrades the response time of the measurement when implemented within a

the standard closed loop configuration. Finally, proportional-integral feedback is a stable control system for making measurements faster than the open loop response time of these resonators because their dither amplitudes and force induced frequency shifts are relatively small.

The research at Yale was supported in part by the U.S. Army Research Office under grant DAAH04-95-1-0368 and by the Semiconductor Research Corporation under Grant No. 98-LJ-438.

FOOTNOTES

1 P. Gunther, U. Ch. Fischer, and K. Dransfeld, Appl. Phys. B **48**, 89 (1989).
2 K. Karrai and R.D. Grober, Appl. Phys. Lett. **66**, 1842 (1995).
3 K. Karrai and R.D. Grober, Proc. SPIE **2535**, 69 (1995).
4 K. Karrai and R.D. Grober, Proc. SPIE **2535**, 69 (1995).
5 A.G.T. Ruiter, J.A. Veerman, K.O. vanderWerf, Appl. Phys. Lett. **71**(1), 28 (1997).
6 H. Edwards, L. Taylor, W. Duncan, and A.J. Melmed, J. Appl. Phys. **82**(3), 980 (1997).
7 M. Todorovic and S. Schultz, Appl. Phys. Lett. **73**(24), 3595 (1998).
8 G. Nomarski, J. Phys. Radium **16**, 9S (1955) and C. Schönenberger and S. F. Alvarado, Rev. Sci. Instrum. **60**, 3131 (1989).
9 D. Sarid, in *Scanning Force Microscopy* (Oxford University Press, New York 1991).
10 T. D. Stowe, K. Yasumura, T. W. Kenny, D. Botkin, K. Wago and D. Rugar, Appl. Phys. Lett. **71**, 288 (1997). We assume an $\exp[-i2\pi ft]$ time dependence throughout the paper.
11 M. J. Gregor, P. G. Blome, J. Schöfer and R. G. Ulbrich, Appl. Phys. Lett. **68**(3), 307 (1996).
12 K. Karrai and I. Tiemann, unpublished
13 T.R. Albrecht, P. Grutter, D. Horne, and D. Rugar, J. Appl. Phys., **69**, 668 (1991).
14 F. Giessibl, Appl. Phys. Lett. **73**(26), 3956 (1998).
15 W.A. Atia, C.C. Davis, Appl. Phys. Lett. **70**(4), 405 (1997).
16 H. Edwards, ibid
17 A.V. Oppenheim and A.S. Willsky, Signals and Systems (Prentice Hall, New Jersey, 1983) Chapter 11, Problem 9.
18 T.R. Albrecht, P. Grutter, D. Horne, and D. Rugar, J. Appl. Phys., **69**, 668 (1991).

FIGURE CAPTIONS

Fig. 1: The measurement system (a) and system response (b). The tuning fork, *TF*, is driven by a voltage source, V_{in}, which is coupled to *TF* trough a transformer. The center tapped transformer also supplies a 180 degree phase shifted wave form to the variable capacitor so as to cancel the current due to stray parallel capacitance of the tuning fork. The net response is that of a series *RLC* oscillator and is due only to the motion of the quartz resonator. The resulting current is measured as a voltage, V_{out}, across R_g. The response of the circuit V_{out}/V_{in} is shown as a function of frequency in (b). The solid line is a fit to Eq. (1), demonstrating that the tuning fork responds like a series *RLC* resonator and that the bridge circuit nulled the stray parallel capacitance of the tuning fork.

Fig 2: The noise spectrum of the circuit in Fig. 1(a). This data was taken by grounding V_{in}. The solid line is a parameterless fit, as described in the text, using the circuit parameters determined from Fig 1(b). The agreement between data and theory demonstrate that the origin of the noise is both the Johnson noise associated with R_g and the thermal noise of the resonator.

Fig. 3: The behavior of the resonator as a function of the height of the probe above the surface taken in atmospheric conditions. In (a) is the output of the '*X*' channel of the lock-in amplifier as a function of the height of the probe above the surface. Note that this goes to zero as the probe reaches the surface. Also shown is the tunneling current, which we use as an indication of when the probe makes contact with the surface. In (b) is shown f_0 and Q of the resonator as a function of the height of the probe above the surface. This data was taken by positioning the probe open loop at a fixed height above the surface and measuring the response function of the resonator, as in Fig. 1(b). Note that frequency shifting only occurs in the last few nanometers of the approach.

Fig. 4: These figures show the response of the feedback loop to a 1 nm, 100 Hz square wave modulation of the sample-tip height. The input is shown as the solid line and the response is shown as the circles. (b) is an expanded view of (a). The response time of the system is of order 0.5 msec, which is 40 times faster than the open loop resonator.

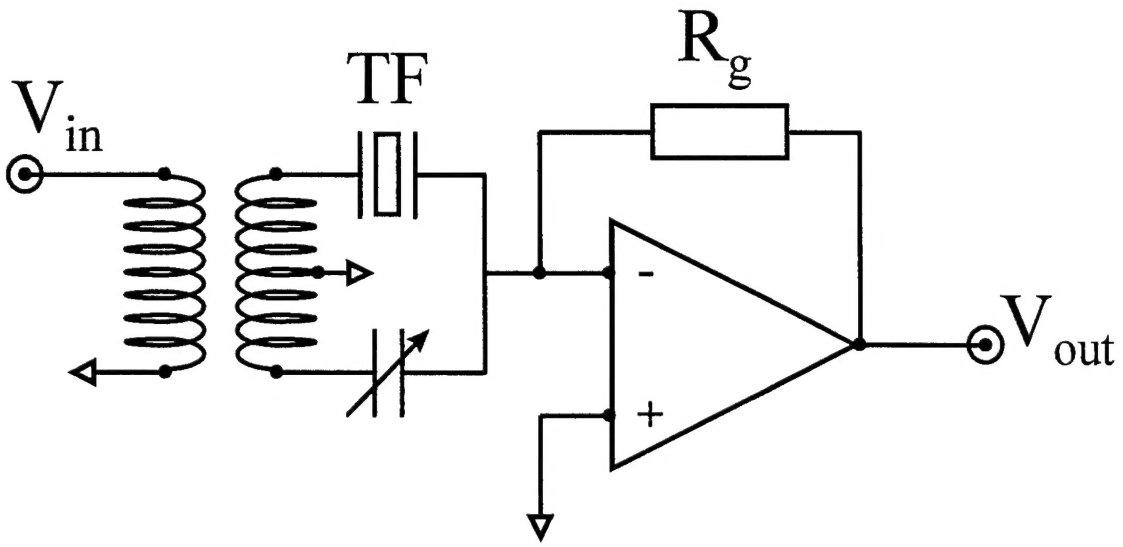
V_{in}
TF
R_g
-
+
V_{out}

Fig. 1(a)

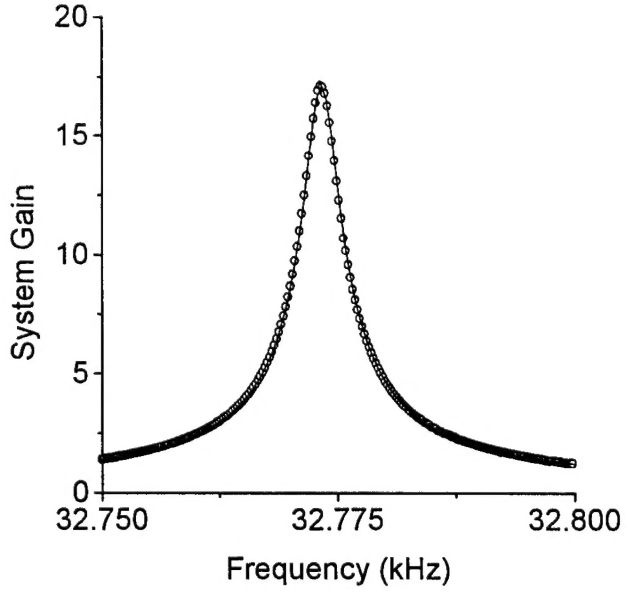
20
15
10
5
0
System Gain
32.750
32.775
32.800
Frequency (kHz)

Fig. 1(b)

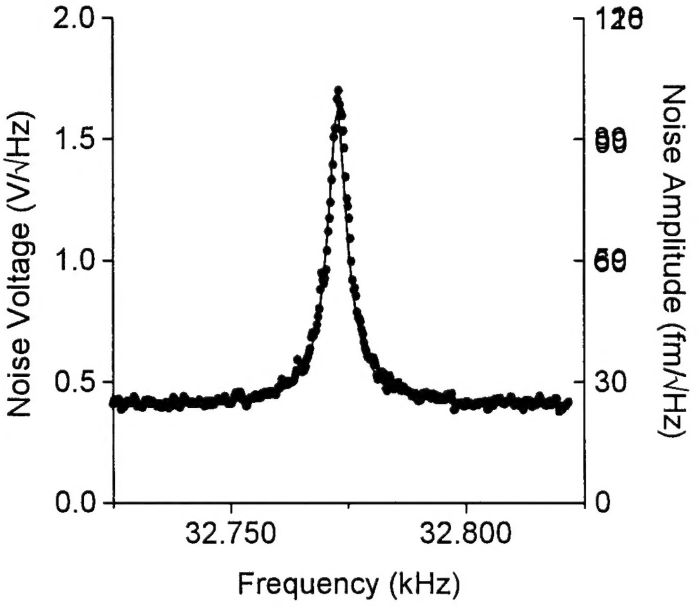
2.0
1.5
1.0
0.5
0.0
Noise Voltage (V/√Hz)
120
90
60
30
0
Noise Amplitude (fm/√Hz)
32.750
32.800
Frequency (kHz)

Fig. 2

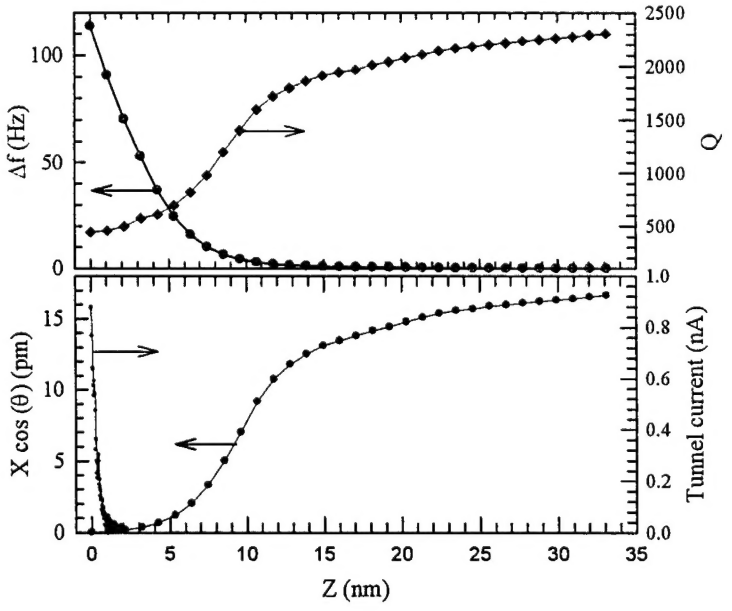
100
50
0
Δf (Hz)
2500
2000
1500
1000
500
1.0
Q
15
10
5
0
X cos (θ) (pm)
0.8
0.6
0.4
0.2
0.0
Tunnel current (nA)
0
5
10
15
20
25
30
35
Z (nm)

Fig. 3

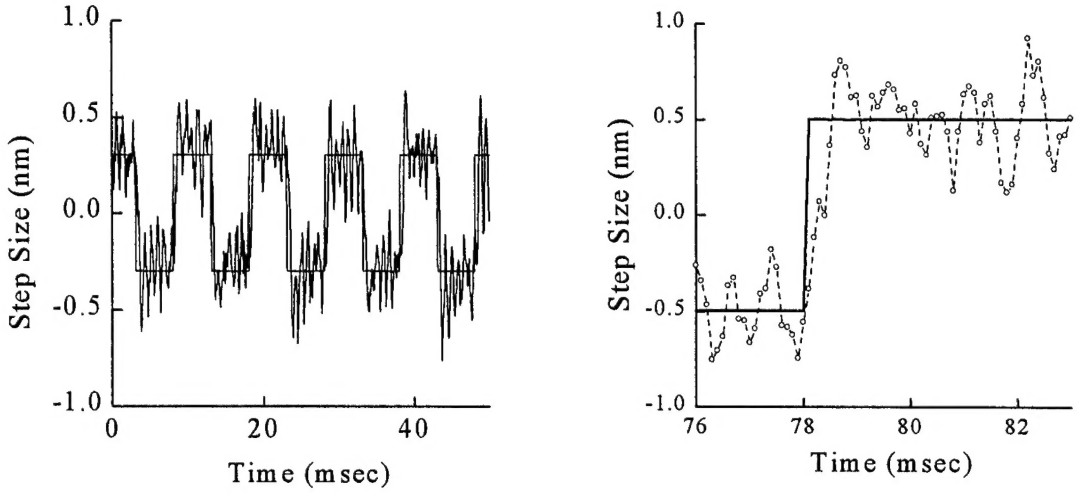
1.0
0.5
0.0
-0.5
-1.0
Step Size (nm)
0
20
40
Time (msec)
1.0
0.5
0.0
-0.5
-1.0
Step Size (nm)
76
78
80
82
Time (msec)

Fig. 4